

The anisotropic thermal expansion of nonlinear optical crystal BaAlBO₃F₂ below room temperature

Xingxing Jiang¹, Naizheng Wang¹, Maxim S. Molokeev², Wei Wang³, Shibin Guo³, Rongjin Huang³, Laifeng Li³, Zhanggui Hu⁴, Zheshuai Lin^{1*}

¹Technical Institute of Physics and Chemistry (CAS), China, ²Laboratory of Crystal Physics, Kirensky Institute of Physics (RAS), Russia, ³Key Laboratory of Cryogenics, Technical Institute of Physics and Chemistry (CAS), China, ⁴Institute of Functional Crystals, Tianjin University of Technology, China

Submitted to Journal:
Frontiers in Chemistry

Specialty Section:
Physical Chemistry and Chemical Physics

Article type:
Original Research Article

Manuscript ID:
389929

Received on:
26 Apr 2018

Revised on:
29 May 2018

Frontiers website link:
www.frontiersin.org

Conflict of interest statement

The authors declare that the research was conducted in the absence of any commercial or financial relationships that could be construed as a potential conflict of interest

Author contribution statement

Xingxing Jiang, Naizheng Wang and Maxim S. Molokeev performed the experiment, Xingxing Jiang performed the first-principles simulation. Wei Wang, Shibin Guo, Rongjin Huang and Laifeng Li help in the variable X-ray diffraction. Zheshuai Lin, Zhanggui Hu and Xingxing Jiang written the manuscript

Keywords

BABF, Anisotropic thermal expansion, phonon stimulation, NLO optical property, Low temperature

Abstract

Word count: 222

Thermal expansion is a crucial factor for the performance of laser devices, since the induced thermal stress by laser irradiation would strongly affect the optical beam quality. For BaAlBO₃F₂ (BABF), a good nonlinear optical (NLO) crystal, due to the highly anisotropic thermal expansion its practical applications are strongly affected by the “tearing” stress with the presence of local overheating area around the laser spot. Recently, the strategy to place the optical crystals in low-temperature environment to alleviate the influence of the thermal effect has been proposed. In order to understand the prospect of BABF for this application, in this work, we investigated its thermal expansion behavior below room temperature. The variable-temperature XRD showed that the ratio of thermal expansion coefficient between along c- and along a(b)- axis is high as 4.5:1 in BABF. The Raman spectrum combined with first-principles phonon analysis revealed that this high thermal expansion anisotropy mainly ascribe to progressive stimulation of the respective vibration phonon modes related with the thermal expansion along a(b)- and c-axis. The good NLO performance in BABF can be kept below room temperature. The work presented in this paper provides an in-depth sight into the thermal expansion behavior in BABF, which, we believe, would has significant implication to the manipulation in atomic scale on the thermal expansion of the materials adopted in strong-field optical facility.

Ethics statements

(Authors are required to state the ethical considerations of their study in the manuscript, including for cases where the study was exempt from ethical approval procedures)

Does the study presented in the manuscript involve human or animal subjects: No

The anisotropic thermal expansion of nonlinear optical crystal

BaAlBO₃F₂ below room temperature

Xingxing Jiang,^{1,5} Naizheng Wang,^{1,5} Maxim S. Molokeev,^{2,6,7} Wei Wang,³ Shibin Guo,³ Rongjin Huang³, Laifeng Li,³ Zhanggui Hu*,⁴ and Zheshuai Lin*,^{1,5}

¹Technical Institute of Physics and Chemistry, Chinese Academy of Sciences, Beijing 100190, China.
*e-mail: zslin@mail.ipc.ac.cn.

²Laboratory of Crystal Physics, Kirensky Institute of Physics, Federal Research Center KSC SB RAS, Krasnoyarsk 660036, Russia.

³Key Laboratory of Cryogenics, Technical Institute of Physics and Chemistry, Chinese Academy of Sciences, Beijing 100190, China.

⁴Institute of Functional Crystals, Tianjin University of Technology, Tianjin 300384, PR. China.
*email: hu@mail.ipc.ac.cn

⁵University of the Chinese Academy of Sciences, Beijing 100049, China.

⁶Department of Physics, Far Eastern State Transport University, Khabarovsk 680021, Russia.

⁷ Siberian Federal University, Krasnoyarsk 660041, Russia.

Abstract: Thermal expansion is a crucial factor for the performance of laser devices, since the induced thermal stress by laser irradiation would strongly affect the optical beam quality. For BaAlBO₃F₂ (BABF), a good nonlinear optical (NLO) crystal, due to the highly anisotropic thermal expansion its practical applications are strongly affected by the “tearing” stress with the presence of local overheating area around the laser spot. Recently, the strategy to place the optical crystals in low-temperature environment to alleviate the influence of the thermal effect has been proposed. In order to understand the prospect of BABF for this application, in this work, we investigated its thermal expansion behavior below room temperature. The variable-temperature XRD showed that the ratio of thermal expansion coefficient between along c- and along a(b)- axis is high as 4.5:1 in BABF. The Raman spectrum combined with first-principles phonon analysis revealed that this high thermal expansion anisotropy mainly ascribe to progressive stimulation of the respective vibration phonon modes related with the thermal expansion along a(b)- and c-axis. The good NLO performance in BABF can be kept below room temperature. The work presented in this paper provides an in-depth sight into the thermal expansion behavior in BABF, which, we believe, would has significant implication to the manipulation in atomic scale on the thermal expansion of the materials adopted in strong-field optical facility.

Introduction

Thermal expansion behavior is a crucial performance factor for materials used in lasers, due to its affinity with the ability of the optical outputting¹⁻⁵. Nonlinear optical (NLO) crystal, a type of crystals for laser frequency conversion, has played a key role in the broadening of laser spectrum and become one of the most prevailing branch of optical materials⁶⁻¹⁰. Among the commercial NLO crystals, BaAlBO₃F₂(BABF) crystal, is a very excellent member, and exhibit many superiority over its congeners in the output of laser in 532 and 355nm¹¹⁻¹⁴. As for the practical application of BABF, the optical spot with high-power is usually focused on one point of the crystal, and thus

“tearing” stress resulted from anisotropic thermal expansion would severely affect the beam quality and outputting power. The previous study about the thermal property of BABF revealed that above room temperature, its thermal expansion coefficient along *c*-axis is about eight times of that along *a(b)*-axis, and the strongly anisotropic thermal expansion has been the major disadvantage to restrict its practical application¹³. However, the microscopic mechanism of the thermal expansion anisotropy in BABF has not been investigated. Recently, it is proposed that the thermal effect on the performance of some optical crystal used in laser can be eliminated to some extent below room temperature¹⁵⁻¹⁷, which provide a feasible method to overcome the problem about the thermal effect. However, the thermal expansion behavior of BABF under low temperature has not been investigated yet, and its performance index below room temperature remain unclear. Therefore, it is desirable to perform a study about the thermal expansion to give a comprehensive evaluation on the application prospect below room temperature and elaborate the structure-property relationship of the anisotropic thermal expansion of BABF.

In this work, using variable-temperature X-ray diffraction, the thermal expansion behavior of BABF below room temperature is studied, and the mechanism of the thermal expansion behavior is elaborated by Raman spectrum and first-principles phonon analysis. The optical property below room temperature is also investigated by first-principles calculation. It is elucidated that BABF still exhibit a relatively strong anisotropic thermal expansion below room temperature, but its anisotropy is less prominent than that above room temperature. The optical performance is also slightly improved under low temperature. These result indicates that the performance below room temperature for the laser generation is superior than that above room temperature, and BABF is a potential NLO crystals in cryogenic system.

Experimental and Computational Method.

Sample preparation: Polycrystalline BABF was synthesized through solid-state reaction. Analytically pure BaF₂, Al₂O₃ and B₂O₃ in stoichiometric ratio as the starting materials were mixed homogeneously by agate mortar. The well grinded reactant then was placed into muffle furnace and was heated gradually up to 800°C at the rate of 0.5°C/min with several intermediate careful grinding at 300K, 600K and 800K. After cooling to room temperature, the white powder of target compound was obtained.

Variable temperature X-ray diffraction: Variable temperature X-ray diffraction patterns were recorded from 13K to 300K with the interval of 20K. Each pattern was recorded with Bruker D8 advanced X-ray diffractometer Cu K α radiation (K α 1=1.5406Å and K α 2=1.5443Å) on the finely grounded powder samples. The angular scanning range were set to 10° to 90° with a step of 0.01° and scanning rate 0.5s/step. The crystal structures under different temperature were refined by Rietveld method¹⁸ using TOPAS 4.2 program¹⁹. Based on the refined cell parameters. The thermal expansion coefficient was fitted by the PASCAL software²⁰.

Raman spectrum: The Raman pattern was recorded from 100 to 1500 cm⁻¹ at room temperature, using in Via-Reflex, equipped with a solid state laser with a wavelength of 532 nm. In order to improve the signal to noise ratio of the spectra, 10 integrations were carried out with an integration time of 10 s at a nominal resolution of 1 cm⁻¹ and a precision of 1 cm⁻¹.

First-principles calculation: The first-principles calculation were performed by CASTEP²¹, a plane-wave pseudopotential total energy package based on density functional theory (DFT)^{22, 23}. The functionals developed by Perdew, Burke, and Ernzerhof (PBE)²⁴ in generalized gradient

approximation (GGA)²⁵ form were adopted to describe the exchange-correlation energy. The optimized norm-conserving pseudopotential²⁶ in Kleiman-Bylander²⁷ form were used to model the effective interaction between the valence electrons and atom cores, which allow us to use a small plane basis set without compromising the accuracy required by the calculation. High kinetic energy cutoff of 900 eV and Monkhorst-pack²⁸ k -point mesh spanning less than 0.04 \AA^{-1} in the Brillouin zone were chosen. The vibrational property was calculated by linear response formalism²⁹, in which the phonon frequencies were obtained by the second derivative of the total energy with respect to a given perturbation. The band gaps at variable temperature were predicted by hybridized functionals PBE0 based on the refined structure at respective temperature, and the refractive index and SHG coefficients were calculated by Kramers–Kronig transform based on the electronic transition matrix³⁰ and the software developed by our group based on length-gauge formalism^{9,31}.

Result and discussion

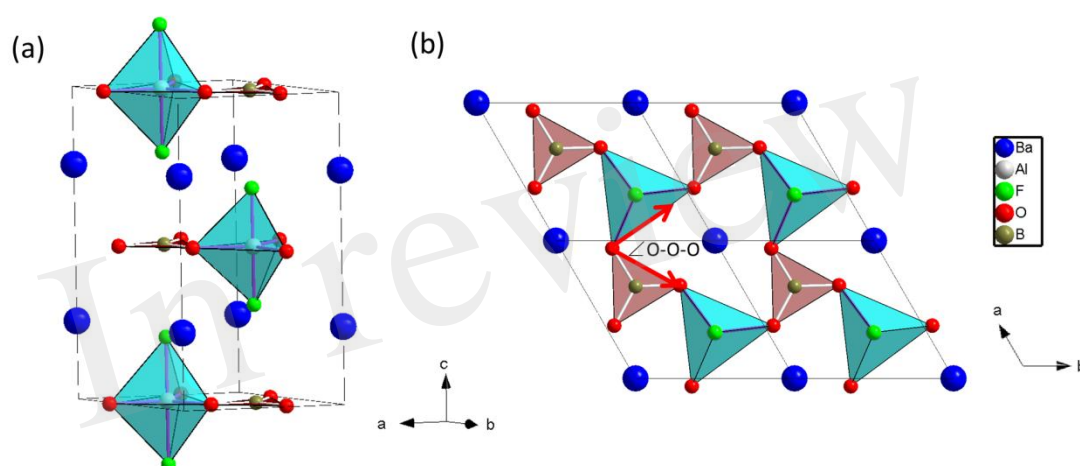


Figure 1 crystal structure of $\text{BaAlBO}_3\text{F}_2$ viewed along (a) (a,b) plane and (b) c -axis. The BO_3 and AlO_3F_2 groups are represented by pink triangles and light blue trigonal bipyramids respectively.

The crystal structure of BABF was determined by Hu *et al*¹². BABF possesses a hexagonal lattice with layered-tendency structure, as displayed in Figure 1. One boron atom is bonded with three oxygen atoms to form a planar BO_3 triangles, and one aluminum atom coordinates with three oxygen and two fluorine atoms to generate the AlO_3F_2 trigonal bipyramid. The BO_3 triangles and AlO_3F_2 trigonal bipyramids are aligned alternatively in the ratio 1:1 by sharing the vertical oxygen atoms, giving rise to the infinite two-dimensional $[\text{AlBO}_3\text{F}_2]_\infty$ layer, in which the BO_3 triangle and the AlO_3 base of AlO_3F_2 trigonal bipyramids are aligned absolutely parallel to (a, b) plane. $[\text{AlBO}_3\text{F}_2]_\infty$ layer are further connected with each other via the Coulomb interaction between the dangling fluorine atoms and interstitial barium atoms to generate the layered-tendency structure.

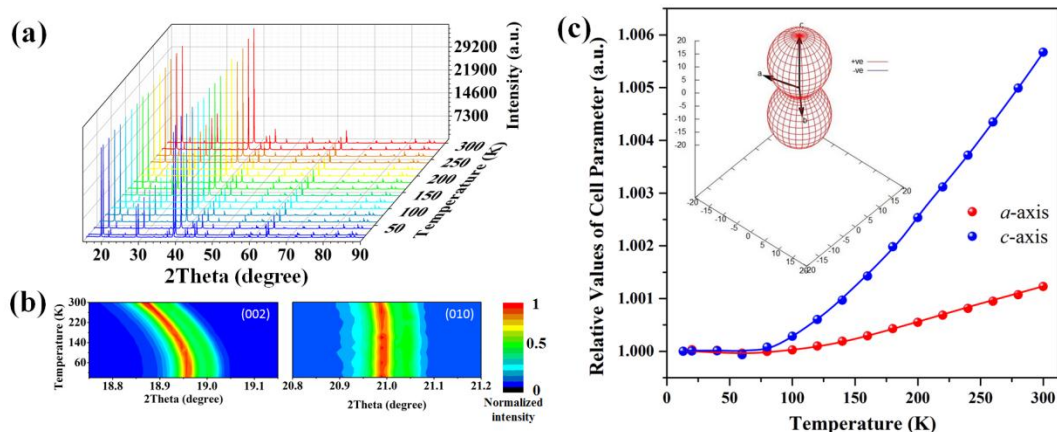


Figure 2 result of VT-XRD on BABF: (a) the VT-XRD patterns, (b) 2θ -temperature contour map of the diffraction peak of (002) and (010) plane and (c) evolution of cell parameters with respect to temperature. The insert in (c) displays the spacial distribution of thermal expansion coefficient plotted by PASCAL software²⁰.

The variable-temperature X-ray diffraction (VT-XRD) patterns are plotted in Figure 2a. It is observed that no new peaks appear as temperature elevate from 13K to 300K, indicating the absence of structural phase-transition and manifesting its high thermodynamical stability. The temperature-deduced diffraction peak-shifting of the lattice plane corresponding to c -axis is much more prominent than that of $a(b)$ -axis (Figure 2b), suggesting the high anisotropic thermal expansion in BABF. According to the cell parameters extracted from the VT-XRD by Rietveld refinement (Figure 2c and table S1), the average thermal expansion coefficient are 4.42(39)/MK and 20.08(71)/MK along $a(b)$ -axis and c -axis respectively, which confirmed that the thermal expansion along c -axis is much more prominent than that along $a(b)$ -axis. More importantly, the ratio (4.5:1) between the thermal expansion coefficients along c - and $a(b)$ -axis below room temperature is much lower than that above room temperature (7.6:1), and the low anisotropy of the thermal expansion below room temperature is more favorable for elimination of the stress induced by temperature gradient when irradiated by laser. Additionally, It should be emphasized that at low temperature (13 to 100K) the $a(b)$ -axis exhibit very low thermal expansion with the fitted linear thermal expansion coefficient 0.11(25)/MK, which is lower than that of c -axis (2.44(98)/MK) by one order and can be categorized to typical zero thermal expansion.

The most intuitive way to investigate the mechanism of the thermal expansion is to trace the modification of bond length and angles with respect to temperature. The $a(b)$ -axis is exclusively determined by B-O, Al-O bonds and \angle O-O-O angle, while c -axis is dominantly determined by the Ba-F and Al-F bond. According to the temperature-dependent bond length and angles (figure 3 and Table S2), despite the clutter of the point due to the difficulty to exactly determine the position of the constituted light atoms in BABF, a roughly changing tendency can be observed. Below 140K the bond length and angles accounting for the change of $a(b)$ -axis almost keep constant, resulting in the rigidity of $a(b)$ -axis under low temperature. And dramatic modification only occur above 140K: B-O bond and \angle O-O-O angle increase from 1.301 to 1.340Å (by 3%) and 60.892° to 62.437° (by 2.5%) respectively as temperature increase from 140K to 300K, which both positively contribute to the thermotropic expansion. Extruded by the increase of \angle O-O-O angle, Al-O bond decrease from 1.919Å to 1.865Å (by 2.8%), which slightly cancel out

the expansion effect originated from the increase of B-O bond and \angle O-O-O angle, leading to the relative low thermal expansion along $a(b)$ -axis. On the contrary, both Al-F and Ba-F bond increase as temperature increase, and thus c -axis exhibit a normal thermal expansion $\sim 10/\text{MK}$ of inorganic crystals.

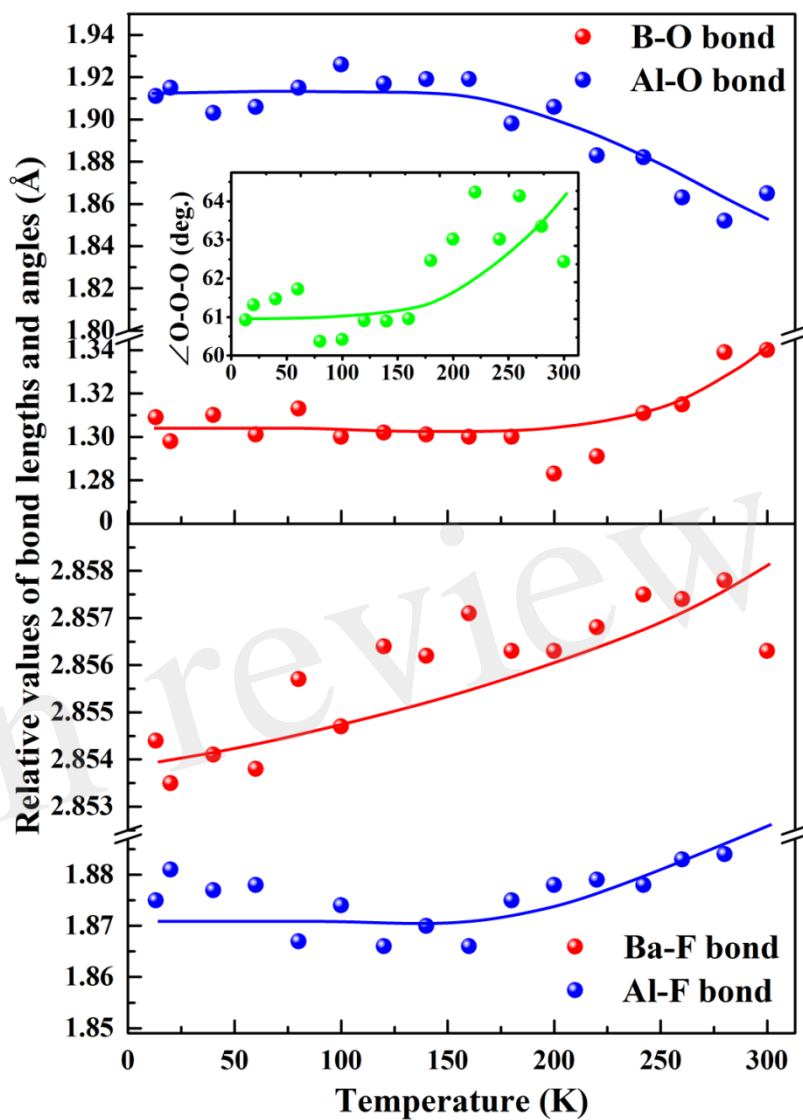


Figure 3 function of refined bond length and angles with respect to temperature in BABF

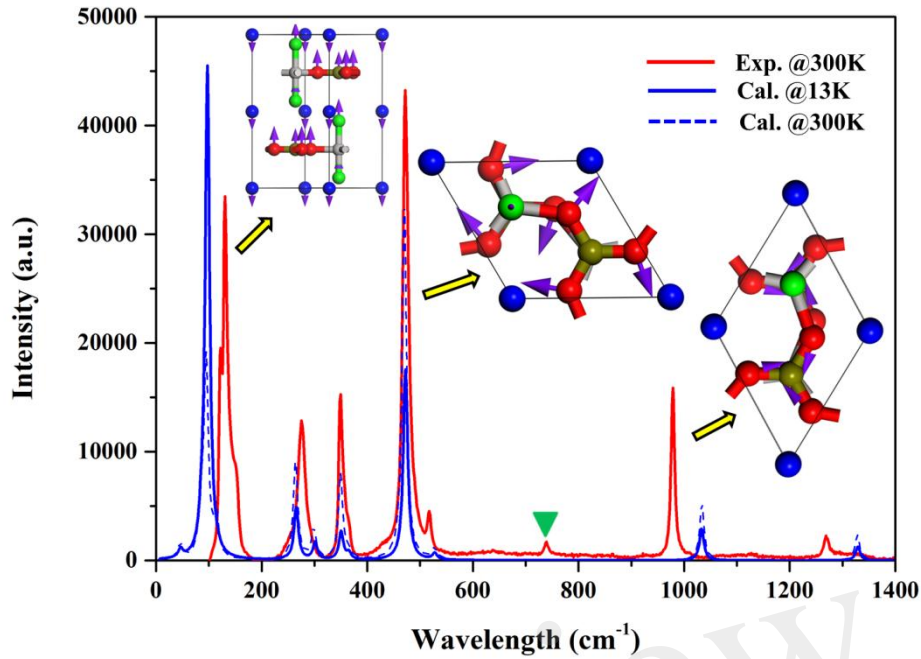


Figure 4 measured and calculated Raman spectrum of BABF. The modes with the highest peaks at 87cm^{-1} , 473cm^{-1} and 1030cm^{-1} are used to schematically describe the atomic vibration of type-I, II and III phonon modes respectively. The peaks at around 720cm^{-1} labeled by green triangle in the experimental spectrum is attributed to the impurity.

The thermal expansion of materials is closely related with the temperature-induced stimulation of lattice vibration, and it is anticipated that first-principles phonon mode assignment would compensate the disadvantage of the littery temperature-dependent bond length and angles and make the mechanism of the thermal expansion in BABF more clear. The irreducible representation of P-62c space group at Γ -point yields a sum of $30E+7A_1+8A_2$ phonon modes (See table S3). According to the calculated Raman spectrum (Figure 4), six principal peaks are observed at around 87cm^{-1} , 266cm^{-1} , 338cm^{-1} , 473cm^{-1} , 1030cm^{-1} and 1331cm^{-1} respectively. The calculated Raman spectrum is in rather agreement with the measured ones, verifying the accuracy of the computational method. According to the vibrational vector projected onto the real space of respective phonon modes, it is revealed that as frequency increase the phonon roughly experience a evolution from the type-I (mode 1 to 7), -II (mode 8 to 29) to -III (mode 30 to 45). In type-I, the configuration of 2D $[\text{AlBO}_3\text{F}_2]_\infty$ layer keep constant and it vibrate as a rigid unit along c -axis with the reverse phase with that of interstitial barium atoms. This indicates that at low temperature the vibration modes related with the stretch between $[\text{AlBO}_3\text{F}_2]_\infty$ and barium would be firstly stimulated, in which the size of $[\text{AlBO}_3\text{F}_2]_\infty$ layer along $a(b)$ -axis remain constant. Therefore, below 100K, BABF exhibit slight thermal expansion along c -axis and rigidity along $a(b)$ -axis. In type-II, the oxygen atoms within $[\text{AlBO}_3\text{F}_2]_\infty$ layer vibrate along the direction almost vertical to B-O bonds. This implies that in these modes, the BO_3 triangles rotate within (a,b) plane as the rigid units. This effect corresponds to the slight contraction of Al-O bond in AlO_3F_2 trigonal

bipyramids and also would lead to the expansion of the interspace within $[\text{AlBO}_3\text{F}_2]_\infty$ layer, which eventually lead to the weak thermal expansion along $a(b)$ -axis. Meanwhile, the stretch vibration of Al-F bonds also partially account for the modes of type-II, which enhanced the thermal expansion along c -axis. In type-III modes, the phonon vibration mainly originate from the stretch of B-O bonds, which is related with the elongation of B-O bonds. It should be emphasized that high temperature is required to stimulate these vibration modes (such as $\sim 1300\text{K}$ for the mode at 1030cm^{-1}), and these modes can only afford the thermal expansion at high temperature and almost contribute nothing to the that below 300K . Moreover, as temperature increase, all the Raman peaks are red-shifted, affording the normal general thermal expansion. Besides, it should be emphasized that the weight of modes related with the thermal expansion along $a(b)$ -axis at 300K is much more prominent than that at 13K , which also result in the enhanced thermal expansion along $a(b)$ axis as temperature increase. Therefore, the anisotropic thermal expansion behavior in BABF is mainly attributed to the progressive stimulation of the respective vibration modes related with the expansion of c -axis to that of $a(b)$ -axis. Moreover, it should be emphasized that as temperature increase, the amplitude of atomic vibration would increase, and the the phonon anharmonicity would be enhanced. Since the thermal expansion is originated from phonon anharmonicity, the thermal expansion of both a -axis ($4.42(39)/\text{MK}$) and c -axis ($20.08(71)/\text{MK}$) between 13K and 300K are less prominent than that those between 303K and 1073K ($6.3/\text{MK}$ and $48.1/\text{MK}$ respectively^[13]).

Additionally, considering that the optical performance is also crucial to the usage in apparatus operated at low temperature, the temperature-dependent optical property was also studied based on the refined structure by first-principles calculation (Figure 5 and Table S4). Accordingly, both the SHG coefficient and birefringence present ultra-stability under temperature fluctuation, and the band gaps are broadened as temperature decrease, which guarantee the optical transmittance of BABF below room temperature. All these observation elucidated that the good optical performance of BABF can be well kept, which is favorable to its practical application in the apparatus operated below room temperature.

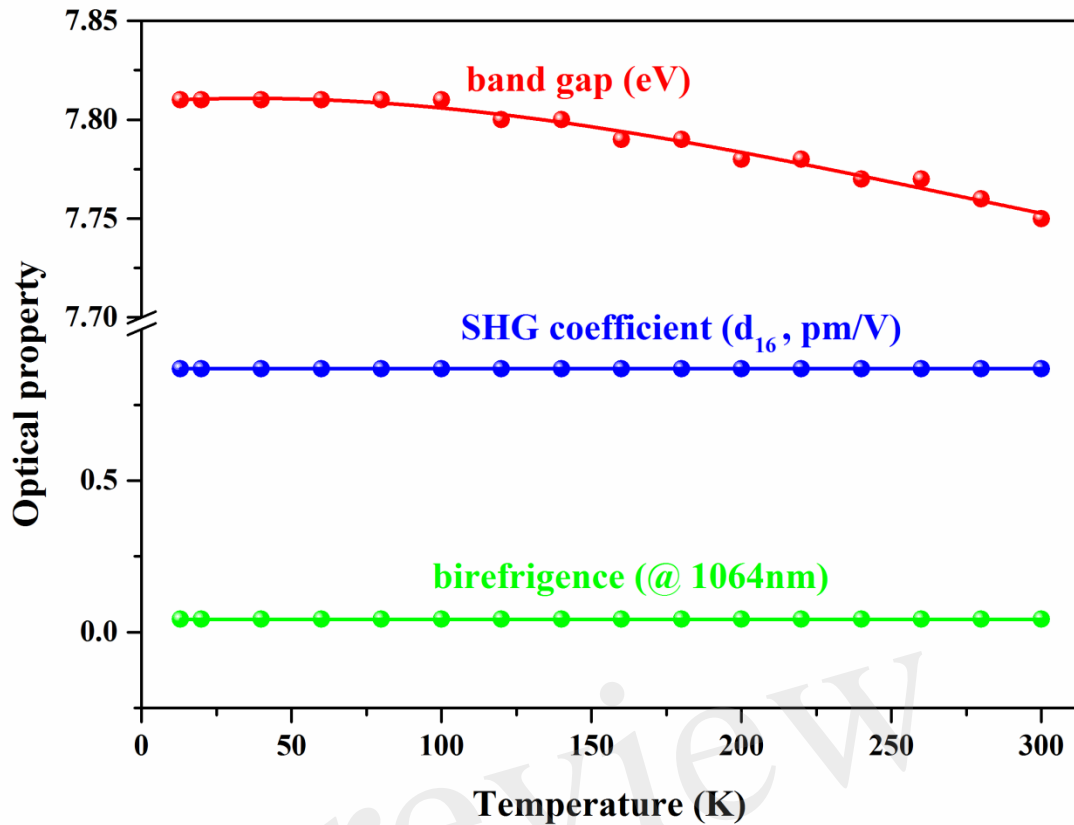


Figure 5 function of the calculated band gap, SHG coefficient and birefringence (@1064nm) of BABF with respect to temperature.

Conclusion

The thermal expansion behavior below room temperature of BABF, an important ultraviolet NLO crystal, is investigated. It is revealed that the BABF exhibit relatively high anisotropic thermal expansion, and the near-zero thermal expansion behavior along $a(b)$ -axis below 100K was observed. Based on the refined temperature-dependent crystal structure, Raman spectrum and first-principles vibration phonon analysis, it is elucidated that the anisotropic thermal expansion behavior in BABF mainly stem from the progressive stimulation of the phonon modes related with the thermal expansion along $a(b)$ - and c -axis. Moreover, it is revealed that the optical performance of BABF can also be well kept under low temperature, which is very favorable for its practical application. Our study exhibit a comprehensive investigation about the thermal and optical property below room temperature and shed light on the structural origin of the thermal expansion of BABF. We believed that the conclusion deduced from our study further deepens the understanding about the performance of BABF and would be beneficial for its practical application under complex environment.

Acknowledgement

This work was supported by the National Scientific Foundations of China (Grants 11474292, 51702330, 11611530680, 91622118, and 91622124), Russian Foundation for Basic Research (Grant 17-52-53031), the Special Foundation of the Director of Technical Institute of Physics and Chemistry (TIPC) and the Youth Innovation Promotion Association, CAS (outstanding member for

Z. Lin and Grant 2017035 for X. Jiang).

Reference.

1. R. Wynne, J. L. Daneu and T. Y. Fan, *Appl. Opt.*, 1999, **38**, 3282-3284.
2. I. Ito, A. Silva, T. Nakamura and Y. Kobayashi, *Opt. Express*, 2017, **25**, 26020-26028.
3. J. Mangin, G. Mennerat and P. Villeval, *J. Opt. Soc. Am. B: Opt. Phys.*, 2011, **28**, 873-881.
4. Z. Wang, Q. Zhang, D. Sun and S. Yin, *J. Rare Earths*, 2007, **25**, 244-246.
5. Z. Fang, L. Liu, X. Wang and C. Chen, *J. Appl. Crystallogr.*, 2018, **51**, 357-360.
6. C. T. Chen, T. Sasaki, R. K. Li, Y. C. Wu, Z. S. Lin, Y. Mori, Z. G. Hu, J. Y. Wang, G. Aka, M. Yoshimura, Y. Kaneda, *Nonlinear Optical Borate Crystals-Principles and Applications*, Wiley-VCH, Germany, 2012.
7. C. T. Chen, N. Ye, J. Lin, J. Jiang, W. R. Zeng and B. C. Wu, *Adv. Mater.*, 1999, **11**, 1071-1078.
8. D. Cyranoski, *Nature*, 2009, **457**, 953-955.
9. Z. Lin, X. Jiang, L. Kang, P. Gong, S. Luo and M.-H. Lee, *J. Phys. D: Appl. Phys.*, 2014, **47**, 253001.
10. J. Meng, G. Liu, W. Zhang, L. Zhao, H. Liu, X. Jia, D. Mu, S. Liu, X. Dong, J. Zhang, W. Lu, G. Wang, Y. Zhou, Y. Zhu, X. Wang, Z. Xu, C. Chen and X. J. Zhou, *Nature*, 2009, **462**, 335-338.
11. L. Yang, Y. Yue, F. Yang, Z. Hu and Z. Xu, *Opt. Lett.*, 2016, **41**, 1598-1600.
12. Z. Hu, Y. Yue, X. Chen, J. Yao, J. Wang and Z. Lin, *Solid-State Sci.*, 2011, **13**, 875-878.
13. Y. Yue, Z. Hu, Y. Zhou, J. Wang, X. Zhang, C. Chen and Z. Xu, *J. Opt. Soc. Am. B: Opt. Phys.*, 2011, **28**, 861-866.
14. Y. Zhou, G. Wang, Y. Yue, C. Li, Y. Lu, D. Cui, Z. Hu and Z. Xu, *Opt. Lett.*, 2009, **34**, 746-748.
15. E. Roitero, M. Ochoa, M. Anglada, F. Muecklich and E. Jimenez-Pique, *J. Eur. Ceram. Soc.*, 2018, **38**, 1742-1749.
16. D. A. Veselov, I. S. Shashkin, Y. K. Bobretsova, K. V. Bakhvalov, A. V. Lutetskiy, V. A. Kapitonov, N. A. Pikhtin, S. O. Slipchenko, Z. N. Sokolova and I. S. Tarasov, *Semicond.*, 2016, **50**, 1396-1402.
17. S. Marrazzo, T. Goncalves-Novo, F. Millet and J.-C. Chanteloup, *Opt. Express*, 2016, **24**, 12651-12660.
18. H. M. Rietveld, *J. Appl. Crystallogr.*, 1969, **2**, 65-71.
19. B. AXS, *Bruker AXS TOPAS V4: General profile and structure analysis software for powder diffraction data. – User's Manual*, Karlsruhe, 2008.
20. M. J. Cliffe and A. L. Goodwin, *J. Appl. Crystallogr.*, 2012, **45**, 1321-1329.
21. S. J. Clark, M. D. Segall, C. J. Pickard, P. J. Hasnip, M. J. Probert, K. Refson and M. C. Payne, *Z. Kristallogr.*, 2005, **220**, 567-570.
22. W. Kohn and L. J. Sham, *Phys. Rev.*, 1965, **140**, 1133.
23. M. C. Payne, M. P. Teter, D. C. Allan, T. A. Arias and J. D. Joannopoulos, *Rev. Mod. Phys.*, 1992, **64**, 1045-1097.
24. J. P. Perdew, K. Burke and M. Ernzerhof, *Phys. Rev. Lett.*, 1996, **77**, 3865-3868.
25. J. P. Perdew and Y. Wang, *Phys. Rev. B*, 1992, **46**, 12947-12954.
26. D. R. Hamann, M. Schluter and C. Chiang, *Phys. Rev. Lett.*, 1979, **43**, 1494-1497.
27. L. Kleinman and D. M. Bylander, *Phys. Rev. Lett.*, 1982, **48**, 1425-1428.
28. H. J. Monkhorst and J. D. Pack, *Phys. Rev. B*, 1976, **13**, 5188-5192.
29. S. Baroni, S. de Gironcoli, A. Dal Corso and P. Giannozzi, *Rev. Mod. Phys.*, 2001, **73**, 515-562.
30. P. E. D, *Handbook of Optical Constants of Solids*, Academic, New York, 1985.

31. J. Lin, M. H. Lee, Z. P. Liu, C. T. Chen and C. J. Pickard, *Phys. Rev. B*, 1999, **60**, 13380-13389.

In review